# *Ab initio* calculation of the $NH(^3\Sigma^-)-NH(^3\Sigma^-)$ interaction potentials in the quintet, triplet, and singlet states

Guillaume S. F. Dhont
*Institute of Theoretical Chemistry, Institute for Molecules and Materials (IMM), Radboud University Nijmegen, Toernooiveld 1, 6525 ED Nijmegen, The Netherlands*

Joop H. van Lenthe
*Theoretical Chemistry Group, Debye Institute, Utrecht University, Padualaan 14, 3584 CH Utrecht, The Netherlands*

Gerrit C. Groenenboom and Ad van der Avoird[a)]
*Institute of Theoretical Chemistry, Institute for Molecules and Materials (IMM), Radboud University Nijmegen, Toernooiveld 1, 6525 ED Nijmegen, The Netherlands*

(Received 24 August 2005; accepted 29 August 2005; published online 7 November 2005)

We present the *ab initio* potential-energy surfaces of the NH–NH complex that correlate with two NH molecules in their $^3\Sigma^-$ electronic ground state. Three distinct potential-energy surfaces, split by exchange interactions, correspond to the coupling of the $S_A=1$ and $S_B=1$ electronic spins of the monomers to dimer states with $S=0$, 1, and 2. Exploratory calculations on the quintet ($S=2$), triplet ($S=1$), and singlet ($S=0$) states and their exchange splittings were performed with the valence bond self-consistent-field method that explicitly accounts for the nonorthogonality of the orbitals on different monomers. The potential surface of the quintet state, which can be described by a single Slater determinant reference function, was calculated at the coupled cluster level with single and double excitations and noniterative treatment of the triples. The triplet and singlet states require multiconfiguration reference wave functions and the exchange splittings between the three potential surfaces were calculated with the complete active space self-consistent-field method supplemented with perturbative configuration interaction calculations of second and third orders. Full potential-energy surfaces were computed as a function of the four intermolecular Jacobi coordinates, with an aug-cc-pVTZ basis on the N and H atoms and bond functions at the midpoint of the intermolecular vector **R**. An analytical representation of these potentials was given by expanding their dependence on the molecular orientations in coupled spherical harmonics, and representing the dependence of the expansion coefficients on the intermolecular distance $R$ by the reproducing kernel Hilbert space method. The quintet surface has a van der Waals minimum of depth $D_e=675\ \mathrm{cm}^{-1}$ at $R_e=6.6a_0$ for a linear geometry with the two NH electric dipoles aligned. The singlet and triplet surfaces show similar, slightly deeper, van der Waals wells, but when $R$ is decreased the weakly bound NH dimer with $S=0$ and $S=1$ converts into the chemically bound $N_2H_2$ diimide (also called diazene) molecule with only a small energy barrier to overcome. © *2005 American Institute of Physics*. [DOI: 10.1063/1.2079867]

## I. INTRODUCTION

The last 15 years have seen great progress in the cooling of neutral atoms in the dilute gas phase. Experiments at ultralow temperatures have succeeded in producing Bose-Einstein condensates of several bosonic atoms[1–4] and, more recently, of fermionic $^{40}K$ atoms.[5] Also molecular condensates[6–9] of $^6Li_2$ and $^{40}K_2$ bosonic molecules have been produced, starting from ultracold $^6Li$ or $^{40}K$ fermionic atoms, via magnetically tuned Feshbach resonances.[10] Methods are being developed to obtain cold molecules without having to first cool the atoms. Paramagnetic atoms or molecules can be trapped and cooled down to a few hundreds of milliKelvins in a magnetic field.[11] The magnetically trapped species are cooled by elastic collisions with a cold helium buffer gas. Another cooling method is to use a Stark decelerator acting on the electric dipole moment of a molecule to slow it down to a near standstill. A magnetic trap or an electrical quadrupole trap can be used for the storage of the molecules, once they are at rest.[12,13]

A promising candidate for directly producing (ultra)cold molecules is NH.[12] The NH molecule in its $^3\Sigma^-$ electronic ground state has both a magnetic dipole moment of two Bohr magnetons and an electric dipole of 1.389 D.[14] In the NH family, $^{14}NH$ and $^{15}ND$ are fermionic whereas $^{15}NH$ and $^{14}ND$ are bosonic. Recent calculations on the collisions of $^{14}NH(^3\Sigma^-)$ molecules with helium atoms[15] have shown that it is theoretically possible to cool the $^{14}NH(^3\Sigma^-)$ molecule with a cold helium buffer gas in a magnetic trap. The very low temperatures required to obtain Bose-Einstein condensation can be obtained, in principle, through an evaporative cooling process by NH–NH collisions. The NH molecules

[a)]Electronic mail: A.vanderAvoird@theochem.ru.nl

 

stay in the trap during this process only if they are in a low magnetic field seeking state, i.e., NH($M_S$=1). A collision dimer consisting of two such molecules is in the NH–NH($M_S$=2) substate of the quintet ($S$=2) state. However, the collisions can change the spin projection $M_S$ of the quintet state, or they can change the total spin $S$ to produce triplet or singlet collision dimers.

An extra complication is that in the singlet and triplet states the two monomers can form the chemically stable $N_2H_2$ molecule. The occurrence of such a deep binding-energy well will probably produce resonant dimer states that are long lived and can form $N_2H_2$ when they get rid of their energy by collision with a third species. Other possible loss channels are the chemical reactions NH+NH→$NH_2$+N and NH+NH→HNN+H, which are both exothermic.[16,17] One of the NH bonds must be broken in these reactions, however, so they probably involve rather high barriers and have very small rates at the low temperatures in the magnetic trap.

A feasibility study of the evaporative cooling process requires the knowledge of the cross sections for elastic and spin-changing NH–NH collisions. These quantities can be theoretically determined by means of time-independent scattering theory, which in turn requires the knowledge of the NH–NH intermolecular potentials in the different spin states. Such a study was previously conducted on $O_2(^3\Sigma_g^-)-O_2(^3\Sigma_g^-)$,[18] with the use of potential surfaces from our group.[19–21] The present paper describes the computation of the four-dimensional NH($^3\Sigma^-$)–NH($^3\Sigma^-$) potential-energy surfaces (PES's) for the quintet, triplet, and singlet states. Section II defines the set of coordinates used to represent the van der Waals complex and gives a brief overview of the electronic structure methods used. Exploratory calculations with valence bond theory are the subject of Sec. III. Section IV is dedicated to the calculation of the full four-dimensional PES's with accurate molecular-orbital (MO)-based quantum chemical methods and to the analytic representation of the *ab initio* computed interaction energies.

## II. ELECTRONIC STRUCTURE OF THE DIMER

According to the Aufbau principle and Hund's rules, the electronic ground state of the NH molecule is a $^3\Sigma^-$ state. Two unpaired $\pi$ electrons are in nonbonding $2p$ orbitals on the N atom and the triplet spin state is associated with the $\pi_x^1\pi_y^1$ or, equivalently, the $\pi_{+1}^1\pi_{-1}^1$ configuration. In the dimer, the electronic spin of monomers $A$ and $B$ couple and the total spin is either a singlet, a triplet, or a quintet. At very large separations these spin states are quasidegenerate. When the wave functions of monomers $A$ and $B$ overlap, the different permutation symmetry of the dimer wave functions imposed by the Pauli principle for the different total spin states leads to different intermolecular exchange effects and the degeneracy is lifted. The most direct way to compute these exchange effects is by the valence bond (VB) method,[22,23] which starts from the many-electron wave functions of the free monomers, imposes the correct many-electron permutation symmetry, and properly deals with the nonorthogonality of the MO's on different monomers. This VB method was used in our first exploratory calculations. Both weak noncovalent interactions and the formation of covalent chemical bonds can be well understood with this method. Refinements of this simple VB treatment allow the relaxation of the monomer MO's in the dimer, either by mixing with MO's on the same monomer or by mixing with MO's on the other monomer as well. We applied the valence bond self-consistent-field (VBSCF) method[24] implemented in the TURTLE program[25,26] as a part of the GAMESS-UK package.[27] With this program it is possible to control the mixing between monomer MO's in the optimization process.

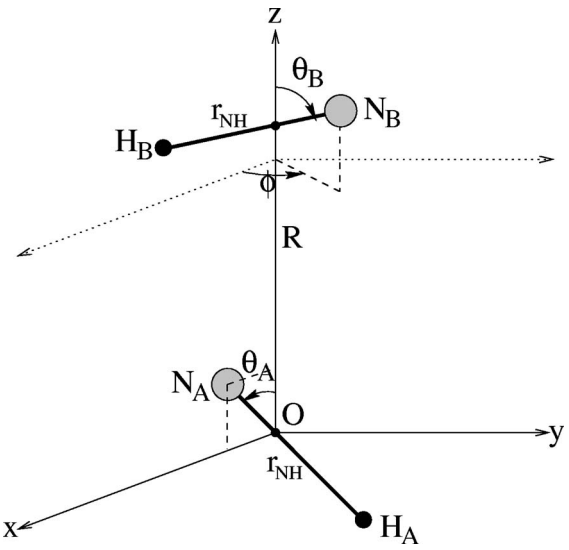


FIG. 1. Coordinates used to describe the NH($^3\Sigma^-$)–NH($^3\Sigma^-$) complex. The $H_AN_A$ diatomic molecule is in the $(O_x,O_z)$ plane. $\theta_A$ and $\theta_B$ are the angles between the axes of the diatomic molecules and the $O_z$ axis. $\phi$ is the dihedral angle between the $(H_BN_B,O_z)$ plane and the $(O_x,O_z)$ plane.

The system under study is expected to be a van der Waals complex with large amplitude motions. Jacobi coordinates are used to describe the geometry of the dimer, see Fig. 1. The NH molecule is treated as a rigid rotor and its bond length was fixed to the experimental equilibrium value[28] $r_e$=1.0362 Å. The potential-energy surfaces depend on the four coordinates: $R$, $\theta_A$, $\theta_B$, and $\phi$. The coordinate $R$ is the length of the intermolecular vector **R** which points from the center of mass of the $H_AN_A$ diatom to the center of mass of the $H_BN_B$ diatom. The angles $\theta_A$ and $\theta_B$ are the angles between the NH monomer axes, pointing from H to N, and the vector **R**. They range from 0 to $\pi$. The $\phi$ coordinate is the dihedral angle between the planes through the vector **R** and the two NH bond axes. This angle take values between $-\pi$ and $\pi$.

The group of feasible permutation-inversion (PI) operations of this complex contains four elements: the identity, space inversion, the simultaneous permutation of the two N and H atoms, and the product of the latter operation with inversion. Equivalent points are described in Table I. This symmetry reduces the computational effort because only points with $\theta_A+\theta_B\leqslant\pi$ and with $\phi$ between 0 and $\pi$ are required.

TABLE I. Equivalent points for a diatom($\Sigma$)-diatom($\Sigma$) potential.

| PI operation | $R$ | $\theta_A$ | $\theta_B$ | $\phi$ |
|---|---|---|---|---|
| $E$ | $R$ | $\theta_A$ | $\theta_B$ | $\phi$ |
| $E^*$ | $R$ | $\theta_A$ | $\theta_B$ | $-\phi$ |
| $P_{AB}$ | $R$ | $\pi-\theta_B$ | $\pi-\theta_A$ | $\phi$ |
| $E^*P_{AB}$ | $R$ | $\pi-\theta_B$ | $\pi-\theta_A$ | $-\phi$ |

Complete four-dimensional PES's were computed with the MOLPRO program[29] by the supermolecule approach. The interaction energy $V$ was computed with the counterpoise correction method of Boys and Bernardi,[30]

$$V(R,\theta_A,\theta_B,\phi) = E_{AB}^{\mathrm{DB}}(R,\theta_A,\theta_B,\phi) - E_A^{\mathrm{DB}}(R,\theta_A,\theta_B,\phi) - E_B^{\mathrm{DB}}(R,\theta_A,\theta_B,\phi). \quad (1)$$

Both the dimer and monomer energies are calculated in the dimer basis (DB). The high-spin quintet state can be described at the Hartree-Fock level with a single Slater determinant and the spin-restricted coupled cluster method with single and double excitations and a perturbative treatment of triples [RCCSD(T)] (Refs. 31 and 32) is employed to recover a large part of the electron correlation energy. The triplet and singlet states have to be described with a multireference wave function and complete active space self-consistent-field (CASSCF) theory followed by second- or third-order perturbation theory [(CASPT2) or (CASPT3)] (Ref. 33) to include excited configurations was used. Also the quintet interaction energies were computed by the latter method, so that we could use the RCCSD(T) results for the absolute interaction energies and the CASPT2 or CASPT3 results for the energy differences between the different spin states. As explained above, these energy differences are determined by short-range exchange (overlap) effects. The long-range electrostatic, induction, and dispersion interactions are probably very similar for the different spin states. The RCCSD(T) method is expected to be better especially for the dispersion interaction.

## III. VALENCE BOND CALCULATIONS

The MO's obtained from a Hartree-Fock calculation of the NH monomer with an aug-cc-pVTZ basis set[34] were used as starting orbitals in our VBSCF calculations. Three variants of VBSCF were considered. In the first variant no optimization of the MO's is performed; the MO's of a monomer cannot adapt to the presence of the other monomer. In the second variant, called VB with optimized monomer orbitals, the MO's of each monomer are allowed to mix with other orbitals on the same monomer only. In the third variant a full optimization of the MO's is performed and the orbitals of each monomer can mix with all other orbitals of both monomers. In all of the VB functions the $\pi_x$ and $\pi_y$ orbitals on both monomers remain singly occupied, so there are four unpaired electrons. Coupling of the $S_A=1$ and $S_B=1$ spin functions of the monomers gives the spin functions for these electrons: $\alpha\alpha\alpha\alpha$ in the quintet ($S=2$) state of the dimer with $M_S=2$, $\alpha\alpha\beta\beta-\beta\beta\alpha\alpha$ for the simplest VB function of the triplet ($S=1$) state with $M_S=0$, and $\alpha\alpha\beta\beta+\beta\beta\alpha\alpha-\frac{1}{2}\alpha\beta\alpha\beta-\frac{1}{2}\alpha\beta\beta\alpha-\frac{1}{2}\beta\alpha\alpha\beta-\frac{1}{2}\beta\alpha\beta\alpha$ for the ($S=M_S=0$) singlet VB function, where $\alpha$ and $\beta$ are the one-electron spin-up and spin-down functions. Each of the spin product functions yields a Slater determinant in the many-electron VB wave function, hence it is clear that only the quintet function can be written as a single determinant.

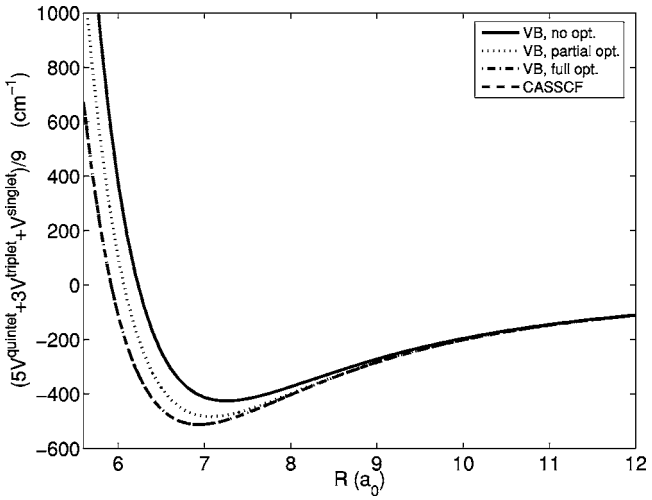


FIG. 2. Weighted average potential $(5V^{\mathrm{quintet}}+3V^{\mathrm{triplet}}+V^{\mathrm{singlet}})/9$ for $\theta_A=\theta_B=\phi=0°$. The valence bond self-consistent-field method was used without optimization, with optimization on monomers only, and with full optimization. The CASSCF calculation corresponds to an active space generated by four electrons in four orbitals. *Ab initio* points were determined for $R=5.7$, 5.9, 6.3, 6.7, 7.1, 7.5, 8.0, 9.0, 10.0, and $12.0a_0$.

In the early papers[21,35] on the $O_2(^3\Sigma^-)-O_2(^3\Sigma^-)$ potentials only the first variant of the VB method was used. The singlet, triplet, and quintet PES's were described by

$$V^S(R,\theta_A,\theta_B,\phi) = \bar{V}(R,\theta_A,\theta_B,\phi) + J(R,\theta_A,\theta_B,\phi) \times \langle S,M_S|\hat{\mathbf{S}}_A\cdot\hat{\mathbf{S}}_B|S,M_S\rangle. \quad (2)$$

The weighted average potential $\bar{V}$ is defined as

$$\bar{V}(R,\theta_A,\theta_B,\phi) = \tfrac{5}{9}V^{S=2}(R,\theta_A,\theta_B,\phi) + \tfrac{3}{9}V^{S=1}(R,\theta_A,\theta_B,\phi) + \tfrac{1}{9}V^{S=0}(R,\theta_A,\theta_B,\phi), \quad (3)$$

and the second term that represents the splitting between the three surfaces contains the so-called Heisenberg Hamiltonian $J\hat{\mathbf{S}}_A\cdot\hat{\mathbf{S}}_B$.[19] The operators $\hat{\mathbf{S}}_A$ and $\hat{\mathbf{S}}_B$ are the spin operators on monomers $A$ and $B$ and the Heisenberg exchange parameter $J$ depends on the intermolecular coordinates. Here we computed the weighted average and the splittings for the NH–NH dimer for two different geometries, a linear one with all the three angles $\theta_A$, $\theta_B$, and $\phi$ equal to zero and a nonlinear one with $\theta_A=40°$, $\theta_B=60°$, and $\phi=90°$.

All of the three VB variants were applied, as well as the CASSCF method with a minimum active space: four electrons in the four half-occupied MO's, denoted as CASSCF(4,4). In Fig. 2 we can see that the more the orbitals can relax the lower is the average energy, as required by the variation principle. The CASSCF(4,4) calculation and the fully relaxed VB result are not distinguishable in this graph. It is easily derived by writing $\hat{\mathbf{S}}_A\cdot\hat{\mathbf{S}}_B=(\hat{S}^2-\hat{S}_A^2-\hat{S}_B^2)/2$ and

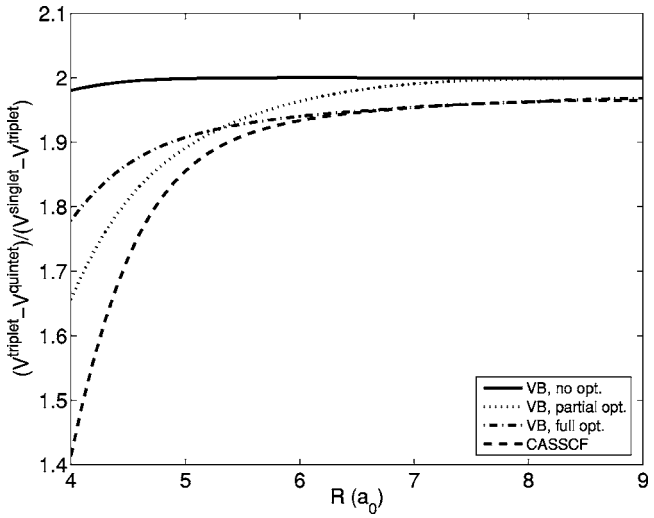


FIG. 3. Ratio $(V^{\text{triplet}}-V^{\text{quintet}})/(V^{\text{singlet}}-V^{\text{triplet}})$ for $\theta_A=\theta_B=\phi=0°$. For details, see Fig. 2. *Ab initio* points were determined for $R$=4.0, 4.5, 5.0, 5.3, 5.7, 5.9, 6.3, 6.7, 7.1, 7.5, 8.0, and $9.0a_0$.

using the fact that the monomer spin functions are eigenfunctions of $\hat{S}_A^2$ and $\hat{S}_B^2$ with $S_A=S_B=1$ that according to Eq. (2) the splitting between the triplet and singlet dimer energies equals $J(R,\theta_A,\theta_B,\phi)$, while the splitting between the quintet and triplet energies equals $2J(R,\theta_A,\theta_B,\phi)$. Hence, if the splittings between the three spin states were given by the Heisenberg Hamiltonian the ratio $r$ defined by

$$r(R,\theta_A,\theta_B,\phi)=\frac{V^{S=2}(R,\theta_A,\theta_B,\phi)-V^{S=1}(R,\theta_A,\theta_B,\phi)}{V^{S=1}(R,\theta_A,\theta_B,\phi)-V^{S=0}(R,\theta_A,\theta_B,\phi)} \quad (4)$$

would be exactly equal to 2 for all geometries. In Fig. 3 we see that this is the case in the first variant with no optimization of the MO's, except for very short distances $R$. However, for the two VB variants with optimized MO's and for the CASSCF calculation the ratio $r$ deviates substantially from 2 and depends more strongly on the dimer geometry. Hence, we should conclude that the differences in the interaction energies of the different spin states cannot be accurately reproduced by the Heisenberg form of Eq. (2). The figures show only the results for the linear geometry with $\theta_A=\theta_B=\phi=0$; the results for the other, nonlinear, dimer geometry for which we obtained VB results are qualitatively similar and support the above conclusion.

In the early studies on the $O_2(^3\Sigma^-)-O_2(^3\Sigma^-)$ dimer it seemed possible to represent the splittings between the three spin states by a Heisenberg Hamiltonian,[19] but we have evidence now that this is no longer accurate when the VB method is improved or when the interaction energies are obtained from another method that allows relaxation of the monomer MO's.

## IV. FOUR-DIMENSIONAL POTENTIAL-ENERGY SURFACES

### A. Active space, basis sets, and grid of geometries

The four-dimensional PES's of the singlet, triplet, and quintet spin states were computed by accurate MO-based methods. The quintet state is a high-spin open-shell state and can be treated by the RCCSD(T) method. The singlet and triplet state must be described by multireference wave functions. We computed the singlet, triplet, and also the quintet state with the CASSCF(4,4) method. The active space is composed of the four orbitals which are half occupied in the quintet state. The dynamic correlation is recovered using the CASPT$n$ method,[33] with $n$ set to 2 or 3. This method is in general nearly but not exactly size extensive.[36] With our active space, the wave functions are linear combinations of the antisymmetrized products of the open-shell Slater determinants describing the two NH molecules in their triplet ground states. The use of the $g_4$ method[37] gives size-consistent results. We faced convergence problems in the perturbation treatment, but this problem disappeared with the use of a shift level equal to 0.4. In either case (coupled cluster or perturbation theory), the frozen-core approximation is used. Usually, a larger fraction of the dispersion energy is recovered from coupled cluster RCCSD(T) calculations than from the perturbation-theory-based CASPT$n$ methods. The exchange terms that are responsible for the splittings between the different spin states are expected to be well reproduced at the CASPT$n$ level. Therefore, we do not use directly the CASPT$n$ energies for the singlet and triplet surfaces, but we obtain these surfaces by adding the splittings between the singlet and triplet states and the quintet state calculated at the CASPT$n$ level to the quintet surface obtained from RCCSD(T),

$$V_n^S=V_{\text{CASPT}n}^S-V_{\text{CASPT}n}^{S=2}+V_{\text{RCCSD(T)}}^{S=2}, \quad (5)$$

with $n$=2 or 3.

The electronic calculations were performed using an aug-cc-pVTZ basis on the N and H atoms,[34] augmented with bond functions located at the midpoint of the intermolecular vector **R** (exponents $s,p$: 0.9, 0.3, and 0.1; $d,f$: 0.6 and 0.2; and $g$: 0.3).

The interaction energies were computed for $R$=4.0, 4.5, 5.0, 5.3, 5.7, 5.9, 6.3, 6.7, 7.1, 7.5, 8.0, 9.0, 10.0, 12.0, 14.0, 16.0, 17.5, 20.0, 25.0, and $30.0a_0$. The angles $\theta_A$ and $\theta_B$ range from 0° to 180° in steps of 20°, and additionally adopt the value of 90°. The $\phi$ angle ranges from 0° to 180° in steps of 22.5°.

### B. Analytic representation of potential surfaces

The PES for each spin $S$ is represented by the following expansion in internal (or body-fixed) dimer coordinates:

$$V(R,\theta_A,\theta_B,\phi)=\sum_{L_A,L_B,L} v_{L_A,L_B,L}(R)A_{L_A,L_B,L}(\theta_A,\theta_B,\phi), \quad (6)$$

with coefficients $v_{L_A,L_B,L}(R)$ depending on $R$. The angular functions are defined as

$$A_{L_A,L_B,L}(\theta_A,\theta_B,\phi)=\sum_{M=-\min(L_A,L_B)}^{\min(L_A,L_B)}\begin{pmatrix}L_A & L_B & L\\ M & -M & 0\end{pmatrix}C_{L_A,M}(\theta_A,\phi_A)C_{L_B,-M}(\theta_B,\phi_B)$$
$$=\sum_{M=0}^{\min(L_A,L_B)}(-1)^M\begin{pmatrix}L_A & L_B & L\\ M & -M & 0\end{pmatrix}A_{L_A,L_B,M}(\theta_A,\theta_B,\phi), \tag{7}$$

where $C_{L,M}(\theta,\phi)$ are the Racah-normalized spherical harmonics, and the difference between the azimuthal angles of the two monomers is the dihedral angle $\phi=\phi_A-\phi_B$. The "primitive" angular functions are

$$A_{L_A,L_B,M}(\theta_A,\theta_B,\phi)=P_{L_A,M}(\cos\theta_A)P_{L_B,M}(\cos\theta_B)\cos M\phi, \tag{8}$$

where $P_{L,M}(\cos\theta)$ are the Schmidt seminormalized associated Legendre functions defined for $M\geqslant 0$ as

$$P_{L,M}(\cos\theta)=\left[(2-\delta_{M,0})\frac{(L-M)!}{(L+M)!}\right]^{1/2}(1-\cos^2\theta)^{M/2}\times\frac{d^M}{d(\cos\theta)^M}P_L(\cos\theta), \tag{9}$$

and $P_L(x)$ are the usual Legendre polynomials defined in Ref. 38. Spherical harmonics are related to these associated Legendre functions as

$$C_{L,M}(\theta,0)=\begin{cases}(-1)^M P_{L,M}(\cos\theta)/\sqrt{2}, & \text{for } M>0\\ P_{L,M}(\cos\theta), & \text{for } M=0\\ P_{L,-M}(\cos\theta)/\sqrt{2}, & \text{for } M<0.\end{cases} \tag{10}$$

It is also possible, of course, to expand the potentials directly in terms of the primitive functions,

$$V(R,\theta_A,\theta_B,\phi)=\sum_{L_A,L_B,M}v_{L_A,L_B,M}(R)A_{L_A,L_B,M}(\theta_A,\theta_B,\phi). \tag{11}$$

We will briefly call this the *LLM* expansion, while Eq. (6) will be called the *LLL* expansion. The *LLL* expansion has the advantage that the coefficients $v_{L_A,L_B,L}(R)$ are invariant under rotation of the coordinate frame. Hence, this expansion can easily be transformed to space-fixed coordinates.

Both expansions are in terms of orthogonal angular functions, and therefore each expansion (or Fourier) coefficient $v_{L_A,L_B,M}(R)$ or $v_{L_A,L_B,L}(R)$ can be looked upon as an overlap integral between the expansion function $A_{L_A,L_B,M}(\theta_A,\theta_B,\phi)$ or $A_{L_A,L_B,L}(\theta_A,\theta_B,\phi)$ and the function to be expanded. This implies that the expansion coefficients can be obtained by numerical integration on a Gauss-Legendre quadrature grid for the angles $\theta_A$ and $\theta_B$, and an evenly spaced grid for $\phi$. For the *LLL* expansion the number of $\phi$ grid points must at least be equal to the number of $\theta_A$ and $\theta_B$ grid points, which number must at least be equal to $\max(L_A,L_B)+1$. For the coefficients of the *LLM* expansion of Eq. (11) the integrals over $\theta_A$, $\theta_B$, and $\phi$ can be carried out independently. The required number of $\phi$ grid points, $\max(M)+1$, is smaller than the number of $\theta_A$ and $\theta_B$ points when the range of $M$ is restricted to be smaller than $\min(L_A,L_B)$. Moreover, the *LLM* expansion is computationally less expensive due to the absence of the summation over $M$ and of the $3j$ symbol in the primitive functions of Eq. (8).

Since for the smallest values of $R$ the potential becomes extremely repulsive for certain orientations of the NH monomers one would need terms with very high values of $L_A$ and $L_B$ in the expansion. To avoid this, the potential was damped in these strongly repulsive regions by means of a tanh function up to a value $V_{\max}$, as in Ref. 39,

$$\tilde{V}=\begin{cases}V, & \text{for } V\leqslant V_0\\ V_0+\beta^{-1}\tanh[\beta(V-V_0)], & \text{for } V>V_0,\end{cases} \tag{12}$$

where $\beta\equiv[V_{\max}-V_0]^{-1}$. With this scheme, the damped potential $\tilde{V}$ is continuous around $V_0$ up to the second derivative. Care was taken to use sufficiently high values of $V_0$ and $V_{\max}$, so that the potential was affected only in regions that are not of any practical importance in bound state and scattering calculations. The actual values used were $V_0=0.1$ $E_h=21\,947.4$ cm$^{-1}$, and $V_{\max}=2V_0$.

After some experimentation with direct least-squares fitting of the expansion to the *ab initio* points, which produced less accurate results, we developed the following procedure. For each value of $R$ on the *ab initio* grid we evaluated the coefficients $v_{L_A,L_B,M}(R)$ in the *LLM* expansion by numerical quadrature of the "overlap integral" of the expansion function $A_{L_A,L_B,M}(\theta_A,\theta_B,\phi)$ and the potential $V(R,\theta_A,\theta_B,\phi)$. For each of the nine equally spaced *ab initio* grid points $\phi$, the potential was first obtained on a $17\times 17$ Gauss-Legendre integration grid in $\theta_A$ and $\theta_B$ by means of a two-dimensional cubic spline interpolation of the $11\times 11$ evenly spaced *ab initio* points $(\theta_A,\theta_B)$. This interpolation method is encoded in the interp2 function of the MATLAB program package.[40] The coefficients $v_{L_A,L_B,M}(R)$ were thus computed for all values of $L_A$ and $L_B$ up to 10 inclusive, and maximum $M$ value equal to 6.

Once the coefficients $v_{L_A,L_B,M}(R)$ in the *LLM* expansion were obtained, the coefficients $v_{L_A,L_B,L}(R)$ in the *LLL* expansion were computed from the equation,

$$v_{L_A,L_B,L}(R)=(2L+1)\sum_{M=0}^{\min(L_A,L_B)}(-1)^M(2-\delta_{M0})\times\begin{pmatrix}L_A & L_B & L\\ M & -M & 0\end{pmatrix}v_{L_A,L_B,M}(R). \tag{13}$$

This equation follows from the "inversion" of Eq. (7), with

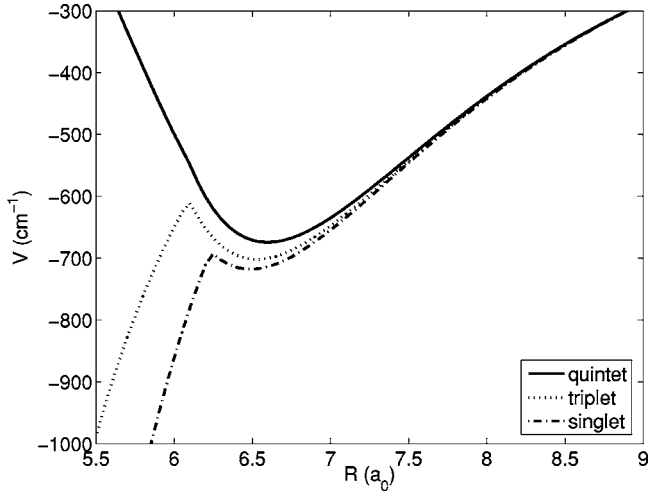


FIG. 4. Minimum of the quintet, triplet, and singlet surfaces $V^{S=2}$, $V_2^{S=1}$, and $V_2^{S=0}$ as a function of $R$, obtained by scanning over the angles $\theta_A$, $\theta_B$, and $\phi$ for each value of $R$.

the use of the known properties of $3j$ symbols.[38] The expansion coefficients $v_{L_A,L_B,L}(R)$ vanish unless $L_A+L_B+L$ is even. It should be noted that for given $L_A$ and $L_B$, the number of $L$ values with even $L_A+L_B+L$ allowed by the triangular relation is equal to the number of non-negative $M$ values.

Finally, the angular expansion coefficients $v_{L_A,L_B,L}(R)$ were fitted as functions of $R$ by means of the reproducing kernel Hilbert space (RKHS) method[41,42] with the reproducing kernel for distancelike variables. The dominant ($\propto R^{-3}$) contribution to each of the potentials $V^S$ in the long range is given by the dipole-dipole interaction with $L_A=L_B=1$ and $L=2$. All contributions with $L=L_A+L_B$ and $L<5$, which decay slower than the leading induction and dispersion terms $\propto R^{-6}$, were fitted with RKHS parameter $m=L_A+L_B$, so that they decay as $R^{-L_A-L_B-1}$ (Refs. 41 and 42) beyond the outermost grid point. All expansion coefficients with $L\neq L_A+L_B$ or $L_A+L_B+1\geqslant 6$ were fitted with RKHS parameter $m=5$ and decay as $R^{-6}$ for very large $R$. The smoothness parameter $n$ was always 2.

In order to test the accuracy of the analytic representation we computed 300 additional arbitrarily chosen *ab initio* points. The difference between the representation and the *ab initio* values is about 0.7% on average, relative to the mean absolute value of the potential in a given distance range (with ranges of $1a_0$). Only for the shortest distance range from 4 to $5a_0$, where the potential becomes extremely anisotropic, the error in the angular expansion becomes larger: 4%–5%.

As shown by Eq. (5) the potential of the quintet state was directly derived from RCCSD(T) calculations, while for the singlet and triplet states the potentials were obtained from the quintet potential by adding the exchange splittings obtained from both CASPT2 and CASPT3 calculations. All of these five potentials were represented analytically. The

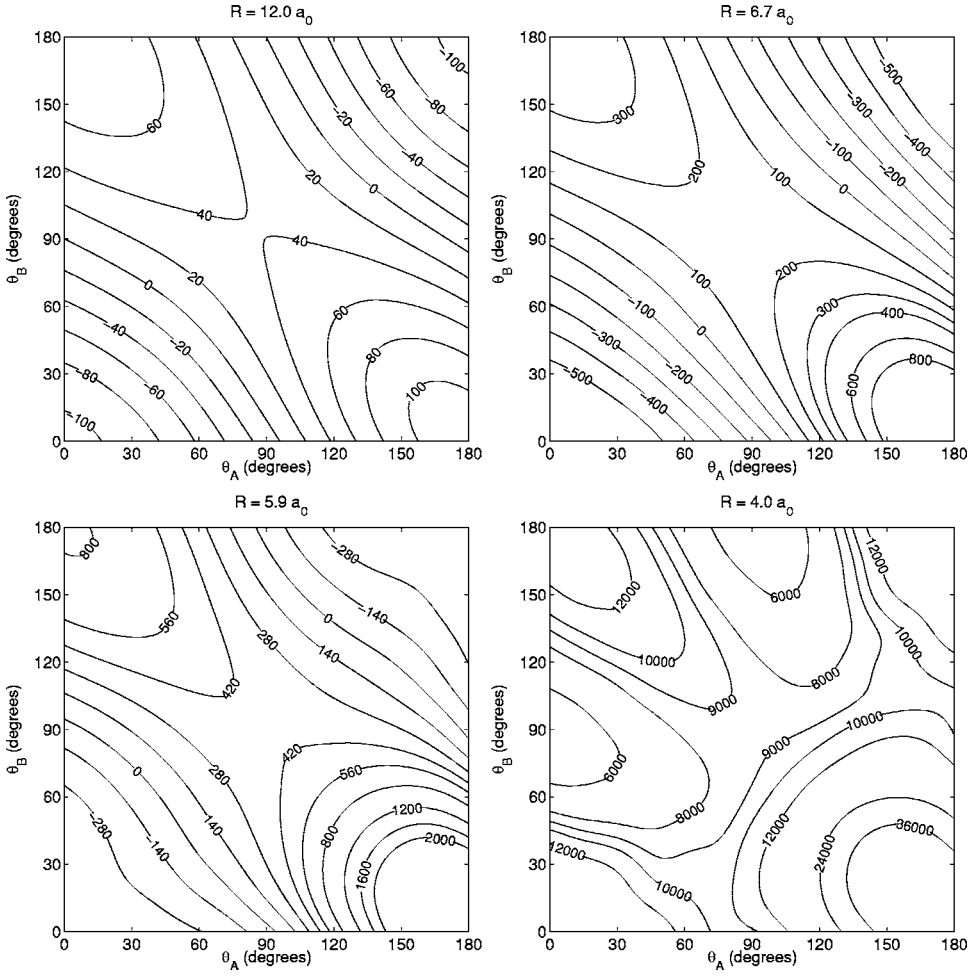


FIG. 5. Cuts of the quintet potential-energy surface $V^{S=2}$ (in cm$^{-1}$) for $\phi=0°$ and different values of $R$.

TABLE II. Characteristics of van der Waals minima and transition states.

| | $R$ ($a_0$) | $\theta_A$ (°) | $\theta_B$ (°) | $\phi$ (°) | Energy ($cm^{-1}$) |
|---|---|---|---|---|---|
| | | van der Waals minimum | | | |
| Quintet | | | | | |
| $V^{S=2}$ | 6.60 | 0 | 0 | 0 | −675 |
| Triplet | | | | | |
| $V_2^{S=1}$ | 6.53 | 0 | 0 | 0 | −702 |
| $V_3^{S=1}$ | 6.53 | 0 | 0 | 0 | −700 |
| Singlet | | | | | |
| $V_2^{S=0}$ | 6.49 | 0 | 0 | 0 | −718 |
| $V_3^{S=0}$ | 6.50 | 0 | 0 | 0 | −714 |
| | | Transition state | | | |
| Triplet | | | | | |
| $V_2^{S=1}$ | 6.09 | 48 | 39 | 180 | −609 |
| $V_3^{S=1}$ | 6.04 | 52 | 43 | 180 | −586 |
| Singlet | | | | | |
| $V_2^{S=0}$ | 6.17 | 39 | 31 | 180 | −660 |
| $V_3^{S=0}$ | 6.13 | 43 | 35 | 180 | −635 |

FORTRAN codes of the fitted potentials are available from the authors upon request.

### C. Results

A first impression of the potential-energy surfaces of all spin states is obtained by plotting the lowest energy obtained by scanning over the angles $\theta_A$, $\theta_B$, and $\phi$ for each value of $R$. The result is shown in Fig. 4. The quintet state has the typical shape of the intermolecular potential of a hydrogen bonded complex, with a well depth $D_e=675\ cm^{-1}$ at $R_e=6.60a_0$. The minimum corresponds to a linear geometry with the two NH electric dipoles aligned. Looking also at the potential we can conclude that the behavior of the quintet state is dominated in the long range by dipole-dipole interaction and in the short range by repulsive exchange forces.

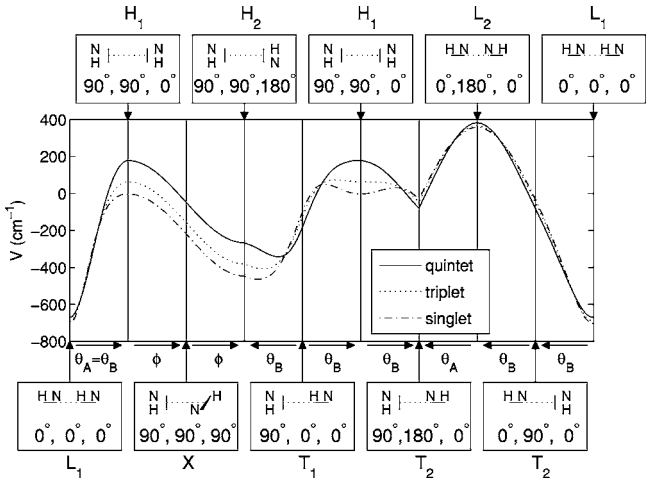


FIG. 6. Orientational dependence of the interaction energies $V^{S=2}$, $V_2^{S=1}$, and $V_2^{S=0}$ (in $cm^{-1}$) of the quintet, triplet, and singlet states for $R=6.7a_0$,

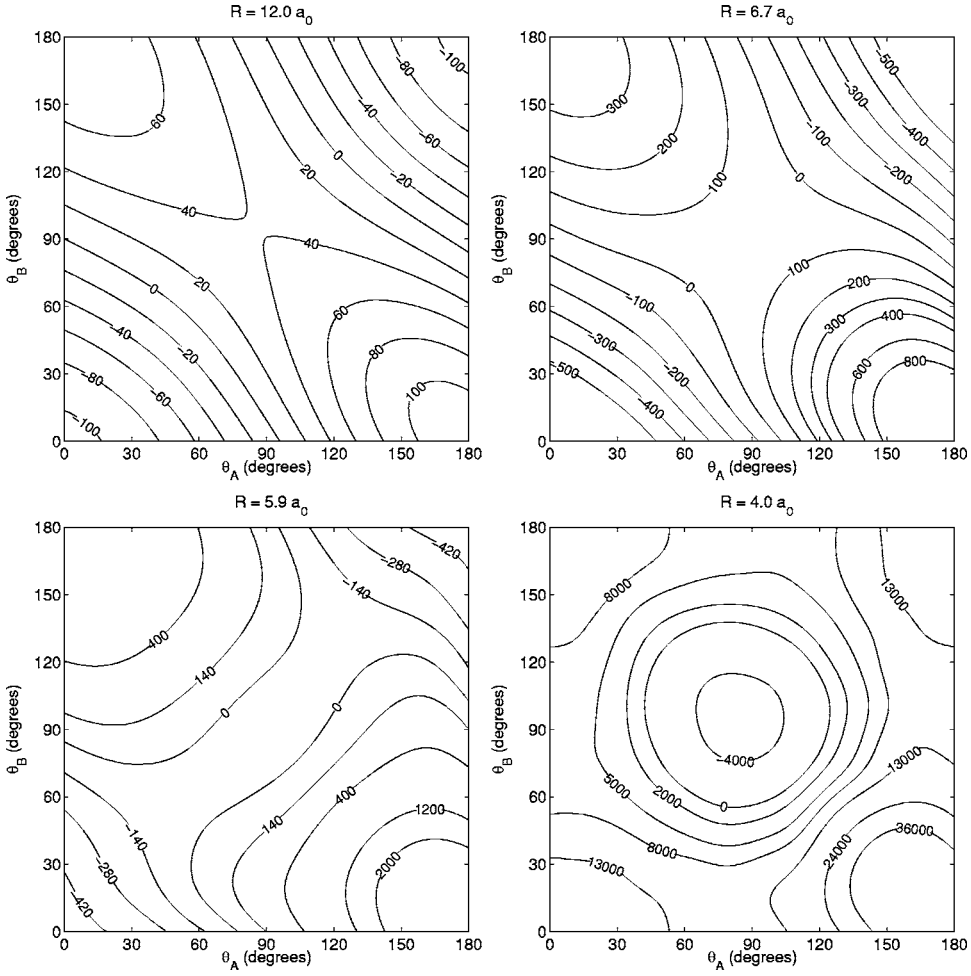


FIG. 7. Cuts of the triplet potential-energy surface $V_2^{S=1}$ (in $cm^{-1}$) for $\phi=0°$ and different values of $R$.

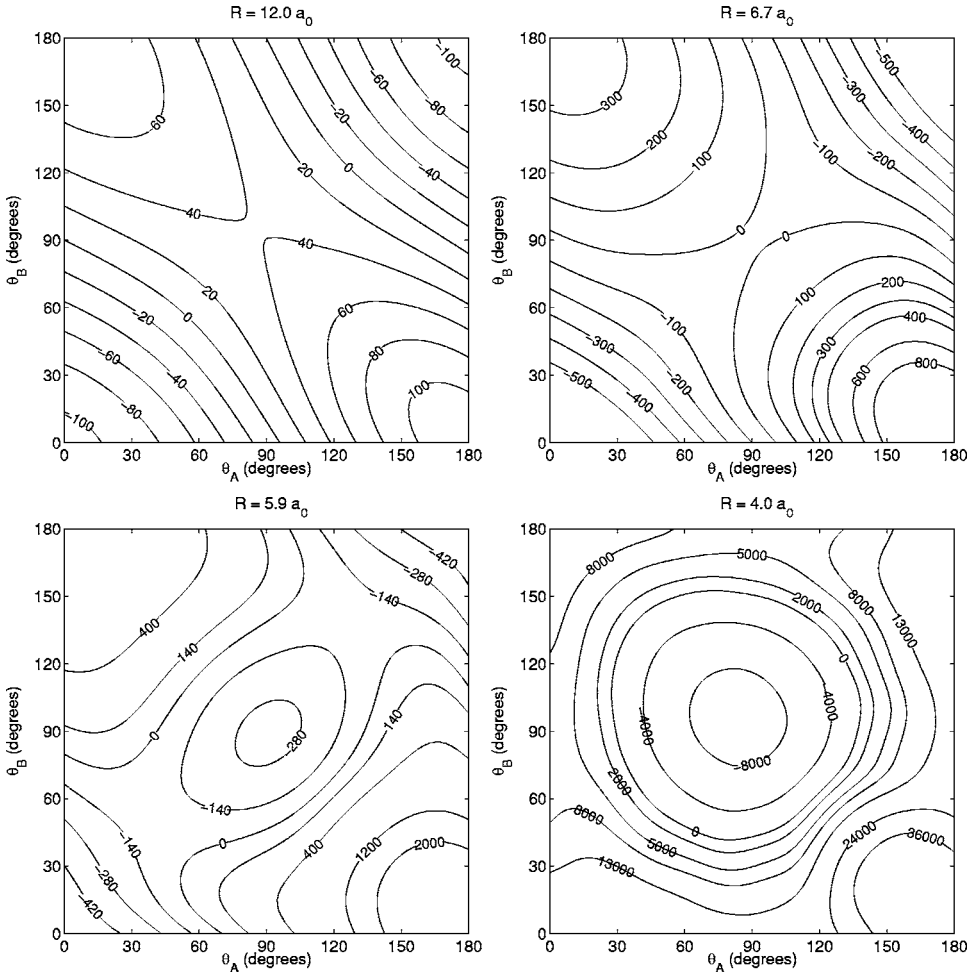


FIG. 8. Cuts of the singlet potential-energy surface $V_2^{S=0}$ (in $cm^{-1}$) for $\phi=0°$ and different values of $R$.

Cuts of the quintet PES at $\phi=0°$ and four intermolecular distances $R$ are given in Fig. 5. For distances larger than $R \approx 6.0a_0$, the minimum is found at linear geometries. At short distances, the anisotropy of the higher multipole electrostatic interactions and of the exchange repulsion become predominant and the minimum corresponds to a nonlinear geometry.

Figure 4 shows that the three spin states nearly coincide for large $R$, but that the exchange interactions cause a splitting between the three surfaces. The characteristics of the van der Waals minima are given in Table II. The binding energies are 675, 700, and 714 $cm^{-1}$ at $R_e=6.60$, 6.53, and $6.49a_0$ for the quintet, triplet, and singlet, respectively. The strongest van der Waals binding always occurs for the linear NH–NH dipole-aligned geometry. For most orientations of the NH monomers the singlet is the most stable and the quintet is the least stable, see Fig. 6, but for specific geometries this energy order is reversed. The latter happens for T-shaped dimers, for example.

The potentials of the singlet and triplet states obtained from the CASPT2 and CASPT3 methods are not very different. This is illustrated by the $D_e$ values: for the singlet they are 718 and 714 $cm^{-1}$ for CASPT2 and CASPT3, respectively, while the corresponding values for the triplet state are 702 and 700 $cm^{-1}$.

Also the triplet and singlet PES's first become repulsive when $R$ is decreased below $6.5a_0$. At still shorter distances, for $R$ smaller than $5.5a_0$, the singlet and triplet potentials become strongly attractive, however, for specific orientations of the molecules. This is in contrast to the $O_2(^3\Sigma^-)-O_2(^3\Sigma^-)$ van der Waals complex, where all of the PES's stay repulsive at short distance.[21] Figures 7 and 8 reveal that the strongest binding is obtained for $\theta_A=\theta_B\approx 90°$. For large values of $R$ the singlet and triplet potentials are similar to that of the quintet: the equilibrium structure corresponds to aligned NH dipoles. At short distances the minimum hops to a configuration with both diatoms nearly perpendicular to the intermolecular axis.

The preferred configurations of the singlet and triplet dimers at short distance can be related to the chemically bound HNNH molecule, either called diimide or 1,2-diazene.[43,44] The ground state of this molecule is a trans form, whereas the cis form is about 0.33 eV higher.[44] The triplet state is nonplanar and is 1.98 eV higher than the trans form.[44,45] We optimized the geometries of these isomers at the CASSCF(4,4) level and at the MRCI level (including the Davidson correction), with an aug-cc-pVTZ basis set, but without bond functions. Table III displays the geometries of these isomers. In the short range part of the singlet and triplet intermolecular PES's the two molecules are "on their way" to form a chemically bound $N_2H_2$ molecule. This is confirmed by Fig. 9, where the $\phi=180°$ global minimum corresponds to the trans structure of the singlet, whereas the $\phi=0°$ local minimum corresponds to the cis form of the singlet. The triplet curve has a minimum at $\phi\approx 110°$, which is

TABLE III. Structure of the lowest singlet and triplet states of diimine HNNH and comparison with previous theoretical and experimental results.

| Coordinates | CASSCF(4,4) | MRCI | Ref. 44[a] | Ref. 46 | Expt.[b] |
|---|---|---|---|---|---|
| Singlet trans-diazene | | | | | |
| $r_{NN}$ (Å) | 1.257 | 1.254 | 1.241 | 1.2468 | 1.247 |
| $r_{NH}$ (Å) | 1.011 | 1.030 | 1.013 | 1.0281 | 1.029 |
| $\angle_{HNN}$ (°) | 106.9 | 106.1 | 107.5 | 106.17 | 106.3 |
| Singlet cis-diazene | | | | | |
| $r_{NN}$ (Å) | 1.258 | 1.254 | 1.241 | 1.2456 | |
| $r_{NH}$ (Å) | 1.014 | 1.035 | 1.017 | 1.0331 | |
| $\angle_{HNN}$ (°) | 111.7 | 111.7 | 112.6 | 111.88 | |
| Triplet diazene | | | | | |
| $r_{NN}$ (Å) | 1.351 | 1.279 | 1.288 | | |
| $r_{NH}$ (Å) | 1.011 | 1.026 | 1.010 | | |
| $\angle_{HNN}$ (°) | 108.3 | 115.2 | 113.9 | | |
| $\angle_{HNNH}$ (°)[c] | 94.5 | 100.4 | 99.8 | | |

[a]Equilibrium structure found at a CASSCF level with an active space of six electrons distributed in four orbitals and a 6-31+G($d$,$p$) atomic basis set.
[b]Reference 47.
[c]Dihedral angle.

similar to the nonplanar lowest triplet state of the $N_2H_2$ molecule. Note that the N–N distance of the chemically bound $N_2H_2$ species, see Table III, is still considerably shorter, however, than the smallest $R$ value of $4a_0$ for which we show the intermolecular potentials in our figures.

Table II gives also the transition states for the conversion of the singlet and triplet van der Waals dimers into the chemically bound HNNH molecule. They occur for $R \approx 6.1a_0$ for both spin states and they have planar trans geometries with smaller angles $\theta_A$ and $\theta_B$ in the singlet state than in the triplet state. Also the energy barrier is lower for the singlet state than for the triplet state. The differences in the transition state energies between the CASPT3 and CASPT2 potential surfaces are somewhat larger than the corresponding differences in the van der Waals well depths.

## V. CONCLUSION

The three potential-energy surfaces of the NH–NH complex that correlate with two separate NH molecules in their $^3\Sigma^-$ electronic ground state were determined *ab initio* and represented in the form of an expansion in coupled spherical harmonics. The quintet state has a typical hydrogen bonding intermolecular potential with a long-range part dominated by dipole-dipole interactions, and strongly anisotropic exchange repulsion at short range. For the triplet and singlet dimer states the situation is similar in the long- and intermediate-range region; the relatively small differences between the potentials of different spin states are due to exchange interactions. A very strong attraction sets in for the singlet and triplet at short distances, explained by the existence of the diimide molecule. The application of these analytic potential-energy surfaces in calculations of the bound states of the NH–NH dimer is in progress. Calculations of the elastic and inelastic NH–NH scattering cross sections relevant for the feasibility of evaporative cooling of magnetically trapped NH will be performed in the near future.

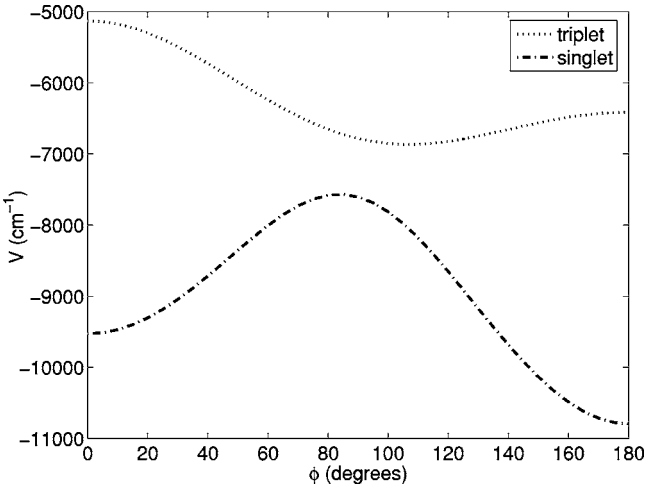


FIG. 9. Minimum of the triplet and singlet surfaces $V_2^{S=1}$ and $V_2^{S=0}$ as a function of $\phi$ for $R=4.0a_0$, obtained by scanning over the angles $\theta_A$ and $\theta_B$ for each value of $\phi$.

## ACKNOWLEDGMENTS

We thank Dr. Paul E.S. Wormer for discussions and for sharing parts of his fitting programs, and Mr. Hubert Cybulski and Dr. Jacek Kłos for their computation of the quintet *ab initio* points. This research has been financially supported by the Council for Chemical Sciences of the Netherlands Organization for Scientific Research (CW-NWO). NCF-NWO is acknowledged for providing computer time on the TERAS computer of the SARA Computing and Networking Services.

[1] M. H. Anderson, J. R. Ensher, M. R. Matthews, C. E. Wieman, and E. A. Cornell, Science **269**, 198 (1995).
[2] K. B. Davis, M.-O. Mewes, M. R. Andrews, N. J. van Druten, D. S. Durfee, D. M. Kurn, and W. Ketterle, Phys. Rev. Lett. **75**, 3969 (1995).
[3] C. C. Bradley, C. A. Sackett, J. J. Tollett, and R. G. Hulet, Phys. Rev. Lett. **75**, 1687 (1995).
[4] C. C. Bradley, C. A. Sackett, J. J. Tollett, and R. G. Hulet, Phys. Rev. Lett. **79**, 1170 (1997).
[5] C. A. Regal, M. Greiner, and D. S. Jin, Phys. Rev. Lett. **92**, 040403 (2004).

[6] S. Jochim, M. Bartenstein, A. Altmeyer, G. Hendl, S. Riedl, C. Chin, J. Hecker Denschlag, and R. Grimm, Science **302**, 2101 (2003).
[7] M. Greiner, C. A. Regal, and D. S. Jin, Nature (London) **426**, 537 (2003).
[8] M. W. Zwierlein, C. A. Stan, C. H. Schunck, S. M. F. Raupach, S. Gupta, Z. Hadzibabic, and W. Ketterle, Phys. Rev. Lett. **91**, 250401 (2003).
[9] M. Bartenstein, A. Altmeyer, S. Riedl, S. Jochim, C. Chin, J. H. Denschlag, and R. Grimm, Phys. Rev. Lett. **92**, 120401 (2004).
[10] S. Inouye, M. R. Andrews, J. Stenger, H.-J. Miesner, D. M. Stamper-Kurn, and W. Ketterle, Nature (London) **392**, 151 (1998).
[11] J. D. Weinstein, R. deCarvalho, T. Guillet, B. Friedrich, and J. M. Doyle, Nature (London) **395**, 148 (1998).
[12] S. Y. T. van de Meerakker, R. T. Jongma, H. L. Bethlem, and G. Meijer, Phys. Rev. A **64**, 041401 (2001).
[13] S. Y. T. van de Meerakker, B. G. Sartakov, A. P. Mosk, R. T. Jongma, and G. Meijer, Phys. Rev. A **68**, 032508 (2003).
[14] E. Scarl and F. Dalby, Can. J. Phys. **52**, 1429 (1974).
[15] H. Cybulski, R. V. Krems, H. R. Sadeghpour, A. Dalgarno, J. Kłos, G. C. Groenenboom, A. van der Avoird, D. Zgid, and G. Chałasiński, J. Chem. Phys. **122**, 094307 (2005).
[16] J. A. Pople and L. A. Curtiss, J. Chem. Phys. **95**, 4385 (1991).
[17] L. A. Curtiss, K. Raghavachari, G. W. Trucks, and J. A. Pople, J. Chem. Phys. **94**, 7221 (1991).
[18] A. V. Avdeenkov and J. L. Bohn, Phys. Rev. A **64**, 052703 (2001).
[19] M. C. van Hemert, P. E. S. Wormer, and A. van der Avoird, Phys. Rev. Lett. **51**, 1167 (1983).
[20] P. E. S. Wormer and A. van der Avoird, J. Chem. Phys. **81**, 1929 (1984).
[21] B. Bussery and P. Wormer, J. Chem. Phys. **99**, 1230 (1993).
[22] S. Shaik and P. C. Hiberty, in *Reviews in Computational Chemistry*, edited by K. B. Lipkowitz, R. Larter and T. Cundari (Wiley-VCH, New York, 2004), Vol. 20, p. 1.
[23] G. A. Gallup, in *Theoretical and Computational Chemistry Valence Bond Theory* Vol. 10, edited by D. L. Cooper (Elsevier, Amsterdam, 2002), p. 1.
[24] J. H. van Lenthe and G. G. Balint-Kurti, J. Chem. Phys. **78**, 5699 (1983).
[25] J. Verbeek, J. Langenberg, C. Byrman, F. Dijkstra, J. Engelberts, and J. van Lenthe, TURTLE is a program designed to perform valence bond self consistent field (VBSCF) calculations (Utrecht University, Utrecht, 2001); see http://tc5.chem.uu.nl/ATMOL/turtle/turtle_main.html
[26] J. H. van Lenthe, F. Dijkstra, and R. W. A. Havenith, in *Theoretical and Computational Chemistry Valence Bond Theory* Vol. 10, edited by D. L. Cooper (Elsevier, Amsterdam, 2002), p. 79.
[27] M. F. Guest, I. J. Bush, H. J. J. van Dam, P. Sherwood, J. M. H. Thomas, J. H. van Lenthe, R. W. A. Havenith, and J. Kendrick, Mol. Phys. **103**, 719 (2005).
[28] K. Huber and G. Herzberg, *Molecular Spectra and Molecular Structure*, IV. Constants of diatomics molecules (Van Nostrand Reinhold, New York, 1979).
[29] R. D. Amos, A. Bernhardsson, A. Berning *et al.*, MOLPRO a package of *ab initio* programs version 2002.1 (Stuttgart, Germany, and Cardiff, UK 2002).
[30] S. F. Boys and F. Bernardi, Mol. Phys. **19**, 553 (1970).
[31] P. J. Knowles, C. Hampel, and H.-J. Werner, J. Chem. Phys. **99**, 5219 (1993).
[32] P. J. Knowles, C. Hampel, and H.-J. Werner, J. Chem. Phys. **112**, E3106 (2000).
[33] H.-J. Werner, Mol. Phys. **89**, 645 (1996).
[34] T. H. Dunning, Jr., J. Chem. Phys. **90**, 1007 (1989).
[35] A. van der Avoird and G. Brocks, J. Chem. Phys. **87**, 5346 (1987).
[36] H. J. J. van Dam, J. H. van Lenthe, and P. Pulay, Mol. Phys. **93**, 431 (1998).
[37] This $g_4$ option is to our knowledge, unfortunately nondocumented. The MOLPRO manual states that "$g_4$ makes CASPT2 calculations size extensive for cases in which a molecule dissociates to high-spin open-shell (RHF) atoms."
[38] D. M. Brink and G. R. Satchler, *Angular Momentum*, 3rd ed. (Oxford Science, New York, 1993).
[39] G. W. M. Vissers, G. C. Groenenboom, and A. van der Avoird, J. Chem. Phys. **119**, 277 (2003).
[40] MATLAB 7, (The Math Works, Natick, MA, 2005); see http://www.mathworks.com
[41] T.-S. Ho and H. Rabitz, J. Chem. Phys. **113**, 3960 (2000).
[42] T.-S. Ho and H. Rabitz, J. Chem. Phys. **104**, 2584 (1996).
[43] K. Vasudevan, S. D. Peyerimhoff, R. J. Buenker, W. E. Kammer, and H. Hsu, Chem. Phys. **7**, 187 (1975).
[44] V. Stepanić and G. Baranović, Chem. Phys. **254**, 151 (2000).
[45] K. Kim, I. Shavitt, and J. E. D. Bene, J. Chem. Phys. **96**, 7573 (1992).
[46] J. Martin and P. Taylor, Mol. Phys. **96**, 681 (1999).
[47] J. Demaison, F. Hegelund, and H. Bürger, J. Mol. Struct. **413–414**, 447 (1997).